

Spectral engineering by flexible tunings of optical Tamm states and Fabry–Perot cavity resonance

Xu-Lin Zhang,¹ Jun-Feng Song,^{1,2,4} Jing Feng,¹ and Hong-Bo Sun^{1,3,5}

¹State Key Laboratory on Integrated Optoelectronics, College of Electronic Science and Engineering, Jilin University, 2699 Qianjin Street, Changchun 130012, China

²Institute of Microelectronics, A*STAR (Agency for Science, Technology and Research), 11 Science Park Road, Singapore Science Park II, Singapore 117685

³College of Physics, Jilin University, 2699 Qianjin Street, Changchun 130012, China

⁴e-mail: songjf@ime.a-star.edu.sg

⁵e-mail: hbsun@jlu.edu.cn

Received September 13, 2013; accepted October 2, 2013;
posted October 7, 2013 (Doc. ID 197570); published October 24, 2013

We present a design for spectral engineering in a metal dual distributed Bragg reflector (DBR)-based structure. Optical Tamm states and Fabry–Perot cavity mode, dual windows for light–matter interaction enhancement, can be excited simultaneously and tuned flexibly, including their respective bandwidth and resonant wavelength, due to the variable reflection phase from the outer DBR’s internal surface. The design can find applications in solar cells for light trappings. Via calculations of overall absorptivity, the proposed simpler dual-states-based scheme is demonstrated to be almost as effective as the coherent-light-trapping scheme, owing to the dual-states-induced broader-band absorption enhancement. © 2013 Optical Society of America

OCIS codes: (310.6845) Thin film devices and applications; (230.1480) Bragg reflectors; (260.5740) Resonance; (040.5350) Photovoltaic.

<http://dx.doi.org/10.1364/OL.38.004382>

Light–matter interaction in photonic structures can be enhanced via the excitations of optical resonant states, such as Fabry–Perot (FP) cavity modes [1], surface plasmon polaritons [2], whispering gallery modes [3], and optical Tamm states (OTSSs) [4]. These resonant states have been studied extensively for applications of lasers [5], light emitting devices [6], and solar cells [7]. The performance of such devices can be improved via a process called spectral engineering, in which the resonant states need to be tuned at the desired wavelength region. Conventionally, one resonant state can provide only one window, that is, in one wavelength region, for light–matter interaction enhancement. However, dual or more windows may be required in some applications such as in white-light emitting devices [8], where they should be designed according to at least two emitting peaks. Although simultaneous excitations of higher- and lower-orders of the same state may provide more than one window [9], these windows are correlated and cannot be tuned independently for spectral engineering. Therefore, designs in which two or more states can be excited simultaneously and tuned flexibly should be studied for spectral engineering. Some pioneering works based on multiple resonant states have been proposed such as the studies on hybrid Tamm plasmons [10–12]. These works focus on discovering new states and revealing the physics for specific applications such as strong couplings, whereas we aim to propose a design for spectral engineering associated with related applications.

In this Letter, we present a design for spectral engineering in the structure of planar metal-distributed Bragg reflectors (DBRs). By integrating dual DBRs on the metal consecutively, OTSSs and the FP cavity mode can be excited simultaneously in the wavelength range of interest. We demonstrate that two states can be tuned flexibly to achieve the desired spectral appearance, including the

resonant wavelengths. By deriving the expression of the resonant frequency, the flexible tunings can be attributed to the variable reflection phase from the outer DBR’s internal surface. Next, for a proof-of-concept demonstration, we apply the dual-states-based scheme to solar cells with dual intrinsic absorption peaks for light trappings. The overall absorptivity can be greatly increased by ~35%, which is almost as high as that in the coherent-light-trapping-scheme-based solar cell, owing to the dual-states-induced broader-band absorption enhancement.

A schematic of the studied metal-DBRs structure is depicted in Fig. 1(a), where dual DBRs called DBR1

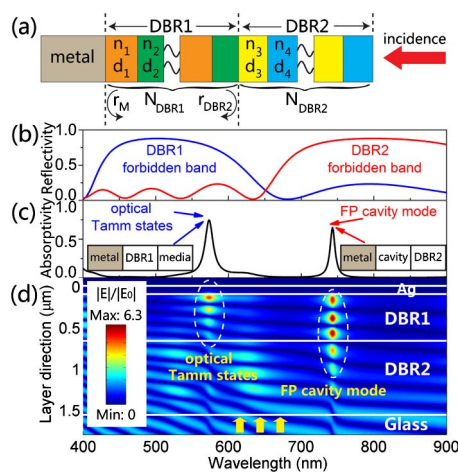


Fig. 1. (a) Schematic of the metal dual DBR-based structure. (b) The reflectivity spectra from air upon each DBR surface. (c) The absorptivity spectrum and (d) the profiles of the electric field intensity enhancement of the metal-DBRs structure. In the calculations, normal TE-polarized incidence is applied, and the structure parameters are chosen as $n_1 = n_3 = 2.2$, $n_2 = n_4 = 1.5$, $\lambda_{B1} = 500$ nm, $\lambda_{B2} = 800$ nm, and $N_{DBR1} = N_{DBR2} = 4$.

and DBR2 are deposited on the metal consecutively. The refractive indices and thicknesses for the DBRs are given by $n_1 \sim n_4$ and $d_1 \sim d_4$, and the DBR pair numbers are denoted by N_{DBR1} and N_{DBR2} , respectively. The DBRs are first considered to satisfy the quarter-wave condition [13] as $\lambda_{B1}/4 = n_1d_1 = n_2d_2$ and $\lambda_{B2}/4 = n_3d_3 = n_4d_4$, where λ_{B1} and λ_{B2} represent the Bragg wavelengths for DBR1 and DBR2, respectively. For simplicity, the refractive indices are chosen as $n_1 = n_3 = 2.2$ and $n_2 = n_4 = 1.5$, and the chosen metal is silver. The silver's permittivity is extracted from the Rsoft package [14] and described by a Lorentzian model with multiple poles. Therefore, the characteristics of the DBRs only depend on the Bragg wavelengths and DBR pair numbers. We first choose $\lambda_{B1} = 500$ nm, $\lambda_{B2} = 800$ nm, and $N_{\text{DBR1}} = N_{\text{DBR2}} = 4$. The reflectivity spectra from air upon each DBR surface for normal TE-polarized incidence are calculated by the transfer matrix method [15] and plotted in Fig. 1(b). We find that the forbidden bands for the two DBRs are interlaced. The purpose of such design is twofold. In the forbidden band of DBR1, with DBR2 considered as conventional media, OTSs at the metal-DBR1 interface [4] can be expected. In the forbidden band of DBR2, DBR1 can be treated as a cavity, inside which an FP cavity mode between metal and DBR2 can be expected.

These expectations can be confirmed by calculating the absorptivity spectrum of the structure shown in Fig. 1(a) for normal TE-polarized incidence. The result is plotted in Fig. 1(c), where dual resonant peaks located at 573 and 744 nm can be observed. To identify these resonant states, the profiles of the electric-field-intensity enhancement $|E|/|E_0|$ (E_0 corresponds to the intensity of incidence) are calculated and shown in Fig. 1(d). We find that OTSs at the metal-DBR1 interface and third-order FP cavity mode in the DBR1 cavity are excited simultaneously in the wavelength range of interest. Significantly, we will show below that the OTSs and FP cavity mode in our designed structure can be tuned flexibly for spectral engineering.

To verify the flexible tunings in our design, we investigate the effect of the DBR pair number and Bragg wavelength on the spectral appearance. We first show in Figs. 2(a) and 2(b) that the bandwidth of the resonant states can be tuned by changing the DBR pair number. Figure 2(a) shows that the bandwidth of the FP cavity mode gets broader with the decrease in N_{DBR2} , while the features of OTSs are barely affected. Meanwhile, we find in Fig. 2(b) that the bandwidth of OTSs gets narrower with the increase in N_{DBR1} , whereas the resonant wavelength of the FP cavity mode shifts to red due to the lengthening of the cavity. The tunings of the resonant bandwidth can be valuable for some applications such as those in solar cells, where broadband resonant states are required for broadband absorption enhancement [16,17].

We then show in Figs. 2(c) and 2(d) that the resonant wavelengths can be tuned by changing the Bragg wavelengths. To achieve the desired spectral appearance, the resonant wavelength of OTSs should first be tuned by changing λ_{B1} . This procedure is shown in Fig. 2(c), from which we also find that the resonant wavelength of the FP cavity mode is also changing due to the variation of

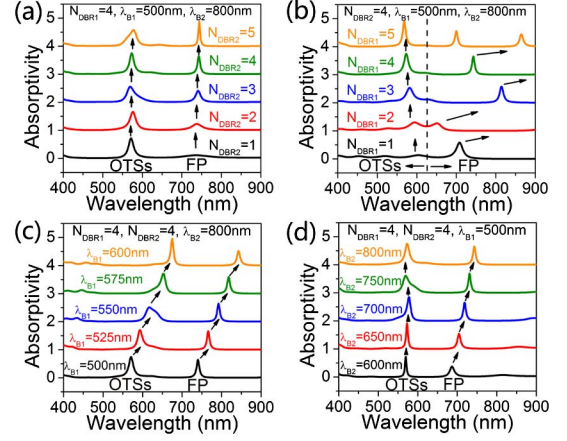


Fig. 2. Variation trends of the absorptivity spectra of the metal-DBRs structure for normal incidence with various values of (a) N_{DBR2} , (b) N_{DBR1} , (c) λ_{B1} , and (d) λ_{B2} . The structure parameters are indicated in each figure.

the cavity length. Once the desired OTS wavelength is achieved, the resonant wavelength of the FP cavity mode can then be tuned by changing λ_{B2} . This step is crucial because we find that in such a procedure, as shown in Fig. 2(d), the resonant wavelength of OTSs would barely be affected, as it only depends on the features of DBR1. Therefore, it can be concluded that in our design the dual resonant states can be tuned flexibly.

Here, for better understanding of the variation mechanism of the FP cavity mode, we derive the expression of its resonant frequency. For instance, we simply take the normal TE-polarized incidence case. The resonance of the FP cavity mode reads

$$\varphi(r_M) + \varphi(r_{\text{DBR2}}) + 2\frac{\omega_{\text{FP}}}{c}N_{\text{DBR1}}(n_1d_1 + n_2d_2) = 2N\pi, \quad (1)$$

where φ demonstrates the phase, r_M and r_{DBR2} are the amplitude reflection coefficients defined in Fig. 1(a), ω_{FP} and c are the resonant angular frequency and vacuum light speed, and N is an integer. By substituting $r_M \approx \exp[i(\pi + (2n_1\omega_{\text{FP}}/\sqrt{\epsilon_b\omega_p}))]$ and $r_{\text{DBR2}} \approx -\exp[i(\pi n_3(\omega_{\text{FP}} - \omega_{B2})/((n_3 - n_4)\omega_{B2}))]$ [4] into Eq. (1), where ω_{B2} , ϵ_b , and ω_p stand for the Bragg frequency of DBR2, infinite frequency permittivity, and plasma frequency of the metal, respectively, the resonant frequency can be obtained as

$$\omega_{\text{FP}} \approx \frac{\frac{\pi n_3}{n_3 - n_4} + (2N - 2)\pi}{\frac{2n_1}{\sqrt{\epsilon_b\omega_p}} + \frac{\pi n_3}{\omega_{B2}(n_3 - n_4)} + \frac{2N_{\text{DBR1}}(n_1d_1 + n_2d_2)}{c}}. \quad (2)$$

From Eq. (2), the variation trends in Fig. 2(d) can be verified as the resonant frequency ω_{FP} is related to the Bragg frequency ω_{B2} . Obviously, this relation comes from $\varphi(r_{\text{DBR2}})$, the reflection phase from the cavity upon the outer DBR's internal surface.

The resonant wavelengths are then extracted and shown in Figs. 3(a) and 3(b), where all the FP cavity

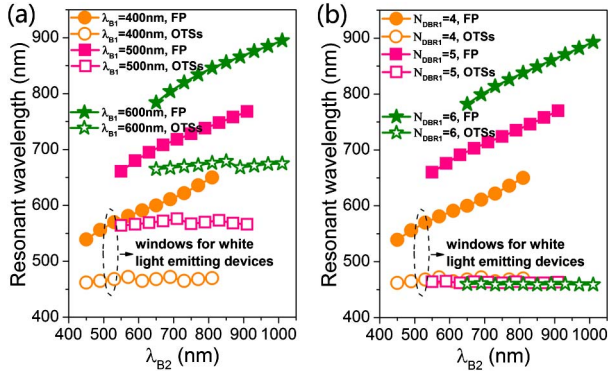


Fig. 3. Resonant wavelengths of OTSs (open symbols) and FP cavity modes (solid symbols) for normal incidence as a function of λ_{B2} with various values of (a) λ_{B1} and (b) N_{DBR1} , where we fix (a) as $N_{\text{DBR1}} = N_{\text{DBR2}} = 4$ and (b) as $\lambda_{B1} = 400$ nm, $N_{\text{DBR2}} = 4$.

modes correspond to the third-order resonances. In Fig. 3(a) with $N_{\text{DBR1}} = N_{\text{DBR2}} = 4$ fixed, we should first choose the desired λ_{B1} for the OTSs, as previously discussed, and then change λ_{B2} for the FP cavity modes. In such a procedure, the OTSs' peaks are nearly invariant. Here, the variation range for FP cavity modes may be slightly small. Fortunately, we show in Fig. 3(b), where $\lambda_{B1} = 400$ nm and $N_{\text{DBR2}} = 4$ are fixed, that the variation range can be considerably enlarged by using different N_{DBR1} [also see Eq. (2)]. In this case, the resonant wavelengths for FP cavity modes are ranging from 540 to 900 nm, while OTSs are always located at around 460 nm. Particularly, by choosing the case (dashed ellipse) with dual peaks located at around 460 and 570 nm, respectively, applications for white-light-emitting devices may be feasible.

Next, as one potential application, we discuss applying the proposed dual-states-based scheme to solar cells for light trappings. As a proof-of-concept demonstration, we study the planar CuPc-PTCBI-based thin-film organic solar cell [17,18] with the structure shown as Device A in Fig. 4(a). Correspondingly, the solar cell with the light-trapping scheme is depicted as Device B, where dual DBRs called DBR-A and DBR-B are inserted between the organic layers and the glass substrate. We first focus on the absorption performance under normal incidence, and the results for TE- and TM-polarized incidence are the same as in planar devices. The absorptivity spectrum in the active layers (CuPc and PTCBI) for Device A is calculated by the transfer-matrix method and shown by the black-dashed line in Fig. 4(b). We find dual intrinsic absorption peaks located at around 615 and 685 nm. Therefore, according to these two intrinsic peaks, light trapping schemes should be designed by exciting OTSs and FP-cavity mode simultaneously.

Following this idea, we study the absorption performance of Device B. The overall absorptivity A_{Total} , which is calculated by $A_{\text{Total}} = (A_{\text{TM}} + A_{\text{TE}})/2$ where $A_{\text{TM,TE}} = (\int_{400}^{900} a_{\text{TM,TE}}(\lambda)S(\lambda)d\lambda) / (\int_{400}^{900} S(\lambda)d\lambda)$, is applied as criteria for the absorption performance of the solar cells [16,–18]. In the equation, $a_{\text{TM,TE}}(\lambda)$ is the absorptivity spectra in the active layers for TM- and TE-polarized incidence, and $S(\lambda)$ is the solar irradiance spectrum under AM1.5 illumination. The refractive indices of the DBRs

are fixed as $n_A = n_C = 1.5$ and $n_B = n_D = 2.2$ in the following calculations. We first choose the DBR pair numbers as $N_{\text{DBR-A}} = 1$ and $N_{\text{DBR-B}} = 2$. The DBRs' thicknesses, not restricted to meet the quarter-wave condition, are then scanned in order to find a maximum of A_{Total} . The obtained thicknesses, which are $d_A = 130$ nm, $d_B = 76$ nm, $d_C = 104$ nm, and $d_D = 128$ nm, are considered as the optimized structure parameters for Device B. The absorptivity spectrum in the active layers for Device B is shown in Fig. 4(b) by the solid line. Compared with that for Device A (dashed line), significant absorption enhancement can be found around the dual intrinsic absorption peaks. From the profiles of the electric field intensity enhancement shown in Fig. 4(c), the absorption enhancement can be attributed to the simultaneous excitations of OTSs (red-dashed line) and the FP cavity mode (green-dashed line) [17]. By introducing the dual-states-based light-trapping scheme, the overall absorptivity for Device B is as high as ~ 0.2106 , which is $\sim 35\%$ higher than that for Device A (~ 0.1556). The overall absorptivity as a function of the incident angle is also calculated and plotted in Fig. 5(b). We find the absorption performance deteriorates with the increase in angle, which is due to the mismatching between the resonant states and the intrinsic absorption peaks [17].

Finally, we study the overall absorptivity for Device B with other combinations of $N_{\text{DBR-A}}$ and $N_{\text{DBR-B}}$. The results for normal incidence are summarized in Fig. 5(a), where in each case the DBRs' thicknesses are optimally chosen in order to obtain the maximum A_{Total} . The overall absorptivity for Device A is plotted by the black-dashed line for comparison. To achieve a higher overall absorptivity, less DBR pairs are preferred, which is in accordance with our previous conclusion from the OTSs-based scheme [16,17]. In our opinion, both conclusions are drawn from the demand for broadband absorption in solar cells, and resonant states with broader bandwidth require less DBRs pairs. In Fig. 5(a), we also calculate the overall absorptivity with $N_{\text{DBR-A}} = 0$, which corresponds to the results of the solar cells with the OTSs-based light-trapping scheme. It can be concluded intuitively that the proposed dual-states-based scheme

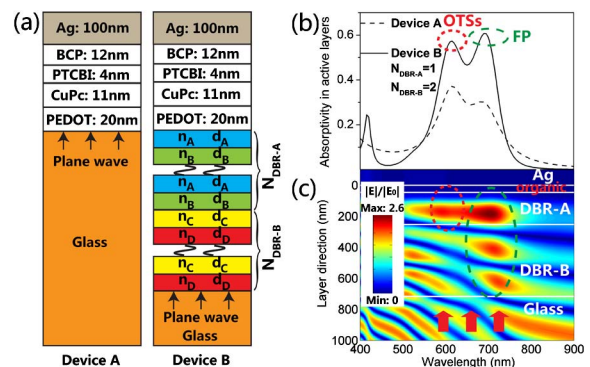


Fig. 4. (a) Schematic of the CuPc-PTCBI based organic solar cells. Device A corresponds to a reference solar cell, and Device B is one with the proposed dual-states-based light trapping scheme. (b) The absorptivity spectra in the active layers for Device A and Device B. (c) The profiles of the electric field intensity enhancement for Device B. In these calculations, normal TE-polarized incidence is applied.

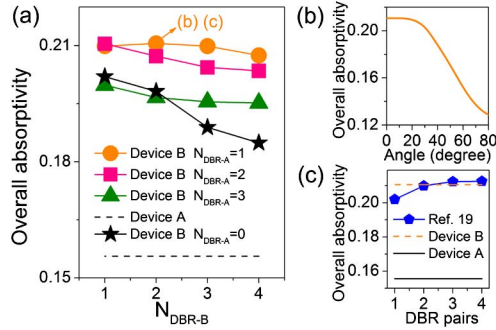


Fig. 5. (a) Overall absorptivity for normal incidence in Device A and Device B with various combinations of $N_{\text{DBR-A}}$ and $N_{\text{DBR-B}}$. In each case, the DBRs' thicknesses are optimally chosen in order to obtain the maximum overall absorptivity. (b) The overall absorptivity for Device B [solid circles in (a)] as a function of the incident angle. (c) The overall absorptivity for the device with the coherent-light-trapping scheme proposed in Ref. [19].

is superior to the OTSs-based scheme for light trapping in solar cells, especially in those devices with more DBR pairs. This is due to the fact that the dual-states-based scheme can provide broader-band absorption enhancement than the single-state-based scheme. Here we also calculate the overall absorptivity of the solar cell with the coherent-light-trapping scheme [19], where the alternating refractive indices are chosen to be the same as those in Device B, but the thicknesses are optimized independently. The optimal results are summarized in Fig. 5(c) by Ref. [19] line. We find the device with our proposed simpler dual-states-based scheme (orange-dashed line) performs almost as well as that with the coherent-light-trapping scheme, which is due to the fact that the bandwidth of dual states can be large enough to cover the high absorption wavelength range of the active layers in such thin-film solar cells.

In summary, we have proposed a design for spectral engineering associated with its potential application in solar cells for light trapping. In the design, OTSs and the FP cavity mode can be excited simultaneously in a metal-DBR structure with dual DBRs. The bandwidth and resonant wavelengths of the two states can be tuned flexibly due to the variable reflection phase from the outer DBR's internal surface. The overall absorptivity

in the solar cell with the dual-states-based light-trapping scheme can be greatly increased by 35%, which is almost as high as that in the one with the coherent-light-trapping scheme.

The authors acknowledge the support from NSFC (Grant Nos. 61177090, 61377048, 90923037, 61137001, and 61107024).

References

1. A. D. Kersey, T. A. Berkoff, and W. W. Morey, *Opt. Lett.* **18**, 1370 (1993).
2. W. L. Barnes, A. Dereux, and T. W. Ebbesen, *Nature* **424**, 824 (2003).
3. J. C. Knight, G. Cheung, F. Jacques, and T. A. Birks, *Opt. Lett.* **22**, 1129 (1997).
4. M. Kaliteevski, I. Iorsh, S. Brand, R. A. Abram, J. M. Chamberlain, A. V. Kavokin, and I. A. Shelykh, *Phys. Rev. B* **76**, 165415 (2007).
5. J. F. Ku, Q. D. Chen, R. Zhang, and H. B. Sun, *Opt. Lett.* **36**, 2871 (2011).
6. Y. F. Liu, J. Feng, Y. G. Bi, J. F. Song, Y. Jin, Y. Bai, Q. D. Chen, and H. B. Sun, *Opt. Lett.* **37**, 124 (2012).
7. Y. H. Su, Y. F. Ke, S. L. Cai, and Q. Y. Yao, *Light: Sci. Appl.* **1**, e14 (2012).
8. C. Xiang, W. Koo, F. So, H. Sasabe, and J. Kido, *Light: Sci. Appl.* **2**, e74 (2013).
9. H. C. Zhou, G. Yang, K. Wang, H. Long, and P. X. Lu, *Opt. Lett.* **35**, 4112 (2010).
10. M. Kaliteevski, S. Brand, R. A. Abram, I. Iorsh, A. V. Kavokin, and I. A. Shelykh, *Appl. Phys. Lett.* **95**, 251108 (2009).
11. R. Brückner, M. Sudzius, S. I. Hintschich, H. Fröb, V. G. Lyssenko, M. A. Kaliteevski, I. Iorsh, R. A. Abram, A. V. Kavokin, and K. Leo, *Appl. Phys. Lett.* **100**, 062101 (2012).
12. I. Iorsh, P. V. Panicheva, I. A. Slovinskii, and M. A. Kaliteevski, *Tech. Phys. Lett.* **38**, 351 (2012).
13. P. Yeh, A. Yariv, and C. S. Hong, *J. Opt. Soc. Am.* **67**, 423 (1977).
14. FULLWAVE, Rsoft Design Group, Inc., www.rsoftdesign.com.
15. P. Yeh, *Optical Waves in Layered Media* (Wiley, 1988).
16. X. L. Zhang, J. F. Song, X. B. Li, J. Feng, and H. B. Sun, *Appl. Phys. Lett.* **101**, 243901 (2012).
17. X. L. Zhang, J. F. Song, X. B. Li, J. Feng, and H. B. Sun, *Org. Electron.* **14**, 1577 (2013).
18. C. Min, J. Li, G. Veronis, J. Y. Lee, S. Fan, and P. Peumans, *Appl. Phys. Lett.* **96**, 133302 (2010).
19. M. Agrewal and P. Peumans, *Opt. Express* **16**, 5385 (2008).